eprints@whiterose.ac.uk
https://eprints.whiterose.ac.uk/

Accepted Manuscript

Modelling fracture and delamination in composite laminates: energy release rate and interfacial stress

J.L. Curiel-Sosa, B. Tafazzolimoghaddam, Chao Zhang

Modelling fracture and delamination in composite laminates: energy release rate and interfacial stress

JL Curiel-Sosa[a,b,*], B Tafazzolimoghaddam[a,b], Chao Zhang[a,b,c]

[a]*Department of Mechanical Engineering, University of Sheffield, Sir Frederik Mappin, Mappin St, Sheffield, S1 3JD*
[b]*Computer-Aided Aerospace and Mechanical Engineering Research Group (CA²M), University of Sheffield, Sheffield, UK*
[c]*School of Mechanical Engineering, Jiangsu University, Zhenjiang, China*

Abstract

This article presents an approach for modelling fracture and delamination, based on the partition of finite elements and on the energy release rate due to crack propagation in cross-ply laminates. The energy release rate is implemented within an Extended Finite Element Method (XFEM) framework. This approach is enabling the prediction of delamination propagation without pre-allocating damage zones. No element deletion techniques were used either. Mesh refinement was not needed for the propagation of cracks. Virtual testing of transverse cracks –eventually triggering delamination in cross-ply laminates– is presented to show the technique efficiency. Thus, a maximum energy release rate of $0.9\,kJ/m^2$ is found for a transverse crack within $[0^0, 90^0]_s$ laminate. When maximum energy release rate is reached, delamination in the $\{0^0/90^0\}$ interface is triggered. Furthermore, delamination in a composite double cantilever beam is simulated and presented in some detail. The results were compared with experimental outputs and/or by other numerical means showing an excellent correlation.

Keywords: , A. Laminate, A. Composites, B. Delamination, C. Finite element analysis (FEA), modelling, energy release rate

1. Introduction

There are a number of un-resolved –or partially solved– problems on modelling of composite failure when several types of failure are involved. Among the outstanding problems:

- Interaction of distinct damage modes[1], so-called mixed-modes damage, i.e. the evolution of more than one damage mode, computed simultaneously. During last decades a vast amount of damage modelling based on the Finite Element Method (FEM) has been based on Continuum Damage Mechanics (CDM) integrating distinct damage internal variables [1]. However, those variables are frequently computed independently of each other evolution which is against the natural mechanism of damage in composites. Exceptions to this include the works by Curiel Sosa et al. [2] or by Matzenmiller et al. [3] amongst others. Naturally, CDM fails to represent the discontinuity of the strain field or displacement field associated to cracks.

- Connection of level of damage with fracture. The link between CDM and fracture mechanics is by a great deal outstanding on composite structures failure modelling. Some advances can be referred though, for instance, the works by van Dongen et al. [4], Turon et al. [5], Iarve et al. [6].

- Interaction of interlaminar fracture, i.e. delamination, and intralaminar fracture, e.g. matrix cracking or fibre breakage/kinking, see the works by Zhao et al. [7] or by Abdullah et al. [8].

Potential shortcomings associated to fracture numerical strategies in composites are highlighted next. Re-

---

*Dr EurIng Jose L. Curiel-Sosa

Email address: j.curiel-sosa@sheffield.ac.uk (JL Curiel-Sosa[a,b,])

URL: www.ca2m.group.shef.ac.uk/ (JL Curiel-Sosa[a,b,])

[1]Damage modes are defined herein in a general sense and attending to the scale considered as: matrix cracking (tension and shear), matrix crushing (compression), fibre breakage, fibre kinking, disbonding (matrix-fibre) and delamination.

cent works are dedicated to overcome those draw-
backs as shown below.

Continuum Damage Mechanics models. So far, most
models based on continuum damage mechanics show
an inability to characterize the interaction of the dis-
tinct failure mechanisms involved in composite fail-
ure, i.e. delamination, fibre breakage/kinking, ma-
trix cracking, etc. For instance, the works by [2, 9]
proposed a model in which the degradation of the
stiffness of the laminate is affected for one or more
internal damage variables to track the damage modes
which permits a straightforward mixed-modes dam-
age simulation. The computation is conducted in a
time-marching scheme –explicit FEM– and the ac-
cumulation of the damage modes can be discontin-
ued which permits a closer simulation to what really
occurs in the failure process. However, no disconti-
nuity associated to fracture is modelled. The pos-
sibility of deleting failed finite elements to simulate
cracks is very appealing. The element is immediately
deleted after the material reaches its maximum ma-
terial strength or a similar criterion is fulfilled. Thus,
only a simple stress criterion –or similar– is needed
to pass from a continuum to a discontinuous domain.
However, element deletion strategies has two main
drawbacks:

- The computation of cracks depends upon the fi-
  nite element mesh and, hence, the crack path is
  influenced by mesh topology. Furthermore, one
  failed element does not lose completely its load
  bearing capability in an instant. This can cre-
  ate numerical instability in the solver and may
  potentially abort the programm execution.

- To avoid aggravation of the former point, re-
  meshing seems a natural option. However, this
  would substantially increase the computational
  cost up to a point whereby it is not applicably
  at industrial scale when complicated geometries
  are to be assessed.

Delamination or interlaminar damage. Debris im-
pact or bird strike on laminated aero-structures may
increase interlaminar shear stresses significantly up to
a point that can trigger non-visible –or barely visible–
interlaminar fracture or delamination. Delamination
will reduce sensibly the bending strength and will in-
crease the risk of buckling in an eventual compressive
state of stress. This is a very serious hazard indeed

for the structural integrity of any aircraft. Delami-
nation in composites is still very difficult to predict
reliably by numerical means. Last ten years or so a
number of schemes have been proposed to tackle not
only the problem of initiation but also the propaga-
tion. Delamination progression is sometimes sought
for energy dissipation, e.g. crashworthiness events.
Modelling this development is challenging for several
reasons. Delamination has been traditionally simu-
lated by means of interfacial fracturing techniques, as
reported by Turon et al. [10]. These attempts were
mainly based on a continuum damage framework for
the computation of internal variables which stored
the history of deformation and damage progression.
The discontinuity caused by the delamination was of-
ten modelled by interface elements whereby the in-
terface constitutive law was imposed, see Shi et al.
[11]. One drawback of cohesive or interface elements
is that they need to be pre-allocated not permitting
delamination elsewhere [12, 13]. This is fine for basic
tests but derates in more complex engineering prob-
lems in which the delamination zones are unknown
a priori. The advent of numerical methods that al-
low the description of the cracks independently of the
mesh and without pre-allocating a priori any damage
zones triggered a revolution in the modelling of frac-
ture in general. Amongst these methods are the eX-
tended Finite Element Method (XFEM) and the eX-
tended Isogeometric Analysis (XIGA). Applications
of XFEM to composite structures include [14, 15, 16].
Other so-called partition of unity finite element meth-
ods (PUFEM) such as the Phanton Node Method [17]
are used in the simulation of matrix cracking and de-
lamination, see van der Meer and Sluys [18].

Combined intralaminar and interlaminar damage. In
general, delamination is not an isolated mode of fail-
ure on composite laminates. Frequently, it is ac-
companied by matrix cracking and, at some cases,
fibre breakage or fibre kinking. Transversal crack
initiated at the surface of the laminate and, subse-
quently, triggering delamination between plies has
been modelled by Hallett et al. [12] using delami-
nation elements –or interface elements[2]– in the in-
terface between plies with embedded matrix cracks.
Although the approach assume pre-allocation of the

---

[2]The nomenclature of interface elements is considered in
many works equivalent to cohesive elements. However, there
may be substantial differences regarding the constitutive law
associated to each of them.

2

cracks and inclusion of interface elements in the delamination, the results correlated well with the tension tests conducted on un-notched carbon/epoxy composite specimens (Hexply IM7/8552) with layups $[45_m/90_m/45_m/0_m]_s$ and scaling factor m variable. Recent numerical developments aim to automatically initiate fracture –whatever its nature– and its evolution without pre-allocating the damage zones. Thus, an interesting approach is undertaken by Hu et al. [19] where delamination is assessed via cohesive elements and matrix cracks are modelled with brick elements subjected to splitting via Extended Finite Element Method (XFEM). The nodes of cohesive elements are enriched –XFEM-alike– to simulate the potential interaction between matrix cracks and delamination. Arguably, the location of cohesive elements in the zones prone to delamination –as in [19] or [7]– pre-allocates the damage, although, some elements will not undergo delamination. A combination between cohesive elements and XFEM is proposed by Hu et al. [19]. Migration of delamination with XFEM for UD laminates is presented by Zhao et al. [7].

This paper is organised as follows. Firstly, the numerical framework implemented in a computer programm is presented highlighting those features for modelling fracture in composites. Secondly, the calculation of energy release rates associated to a transverse crack evolving in the 0^0 plies of a cross-ply laminate is presented. Thirdly, the propagation of delamination in a $\{0^0/90^0\}$ interface is shown for a double cantilever beam (DCB) in mode I fracture. Finally, remarks emphasizing the achievements of this investigation are collated in the conclusion section.

2. Numerical Framework for Fracturing Composites

This section offers the formulation of the implemented extended Finite Element Method (XFEM) tailored for simulation of fracture in composites based on energy release rates. Thus, an XFEM for modelling fracture in composites has been coded in MATLAB$^©$ in which every detail is subjected to trial and validation with complete access to the source code. A novel computation of the energy release rate with XFEM is implemented making use of numerical integration of the contour integral in a number of elements surrounding the crack front. The interested reader is referred to Belytschko et al. [20] for a comprehensive overview on XFEM.

The XFEM is based on the use of special enrichment or set of interpolation functions to approximate the displacement field Eq.(1) (or any other unknowns) modelling in that fashion discontinuities such as cracks or interphases. Eq.(2) represents the classical finite element approximation which applies to all elements in the mesh. Eq.(3) shows the additional term in the displacement field to compute a discontinuity such as a jump on the displacement field. Only the elements in the vicinity of a crack are modelled by Eq.(3), i.e. enriched elements and nodes. Thus, the displacement approximation in the vicinity of a crack is affected for this so-called enrichment Eq.(3). The enrichment can be different in the enriched nodes depending upon whether they are on the neighbourhood of the crack tip (2D) –or crack front (3D)– or they are along the faces of the crack. Other types of discontinuities can also be modelled with special enrichment such as interfaces or inclusions, see Ibbett et al. [21].

$$\mathbf{u}(\mathbf{x}) = \mathbf{u}^{(std)} + \mathbf{u}^{(enr)} \tag{1}$$

$$\mathbf{u}^{(std)}(\mathbf{x}) = \sum_{\mathbb{A}\subset\mathcal{N}_{std}} \mathbf{N}^{\mathbb{A}}(\mathbf{x})\mathbf{u}^{\mathbb{A}} \tag{2}$$

$$\mathbf{u}^{(enr)}(\mathbf{x}) = \sum_{\mathbb{B}\subset\mathcal{N}_{enr}} \sum_{k=1}^{m} \psi_k(\mathbf{x})\,\mathbf{N}^{\mathbb{B}}(\mathbf{x})\boldsymbol{a}_{\boldsymbol{k}}^{\mathbb{B}} \tag{3}$$

where $\mathbf{N}^{\mathbb{A}}(\mathbf{x})$ are the standard shape functions that obeys the partition of unity, $\mathcal{N}_{std}$ is the set of all nodes of the mesh, $\mathcal{N}_{enr}$ is the subset of enriched nodes, $\mathbf{N}^{\mathbb{B}}(\mathbf{x})$ are the shape functions used in the enrichment, and $\boldsymbol{a}_{\boldsymbol{k}}^{\mathbb{B}}$ are the additional degrees of freedom –unknowns– in the enriched nodes. $\psi_k(\mathbf{x})$ are the enrichment functions and m denotes the number of them. They can represent the special stress field on the vicinity of crack front, an interphase or be a Heaviside function to represent the jump on the displacement field along the crack faces. In the case of the enrichment function of the crack front, $\psi_k(\mathbf{x})$ are based often in asymptotic solutions which are not exact. In order to solve this shortcoming, Belytschko et al. [22] proposed that the enrichment functions are shifted as performed in Eqs.(5, 6) allowing the product of the enrichment function $\psi_k(\mathbf{x})$ and the shape function $\mathbf{N}^{\mathbb{B}}(\mathbf{x})$ to vanish at every node. Therefore, the Heaviside enrichment along the crack faces vanishes at the element edges which are not crossed by the crack.

3

$$\mathbf{u}^{(enr)}(\mathbf{x}) = \mathbf{u}^{(face)}(\mathbf{x}) + \mathbf{u}^{(front)}(\mathbf{x}) \qquad (4)$$

$$\mathbf{u}^{(face)}(\mathbf{x}) = \sum_{\mathbb{B} \subset \mathcal{N}_{face}} [H(\mathbf{x}) - H(\mathbf{x}_{\mathbb{B}})] \, \mathbf{N}^{\mathbb{B}}(\mathbf{x}) \boldsymbol{d}^{\mathbb{B}} \qquad (5)$$

$$\mathbf{u}^{(front)}(\mathbf{x}) = \sum_{\mathbb{C} \subset \mathcal{N}_{front}} \sum_{k=1}^{m} [\psi_k(\mathbf{x}) - \psi_k(\mathbf{x}_{\mathbb{C}})] \, \mathbf{N}^{\mathbb{C}}(\mathbf{x}) \boldsymbol{b}_{\boldsymbol{k}}^{\mathbb{C}} \qquad (6)$$

where $\mathcal{N}_{face}$ denotes the subset of enriched nodes with Heaviside step function and additional nodal degrees of freedom $\boldsymbol{d}^{\mathbb{B}}$ along the crack faces. $\mathcal{N}_{front}$ is the subset of enriched nodes with asymptotic functions and additional degrees of freedom $\boldsymbol{b}_{\boldsymbol{k}}^{\mathbb{C}}$ on the crack front vicinity. Eq.(4) is rearranged in compact form in Eq.(7) for straightforward obtention of the weak form as explained below.

$$\mathbf{u}(\mathbf{x}) = \mathbf{N}^{\mathbb{A}}(\mathbf{x}) \cdot \mathbf{u}^{\mathbb{A}} + \mathbf{N}^{(enr)}(\mathbf{x}) \cdot \mathbf{a}^{(enr)} \qquad (7)$$

where,

$$\mathbf{N}^{(enr)}(\mathbf{x}) = [\mathbf{N}^{(face)}(\mathbf{x}), \mathbf{N}^{(front)}(\mathbf{x})]$$

and,

$$\mathbf{a}^{(enr)} = [\boldsymbol{d}^{\mathbb{B}}, \boldsymbol{b}^{\mathbb{C}}]$$

with,

$$\boldsymbol{b}^{\mathbb{C}} = [\boldsymbol{b}_{\boldsymbol{1}}^{\mathbb{C}}, ..., \boldsymbol{b}_{\boldsymbol{m}}^{\mathbb{C}}]$$

Asymptotic field ahead of crack front. For orthotropic materials special enrichment functions are used to simulate the mechanical behaviour ahead of the crack front. The enrichment functions given in
220 Eq.(8) are used for orthotropic materials [23]. However, note that the asymptotic field ahead of the crack tip for two-dimensional isotropic materials are also valid for three-dimensional cracks as shown in Wang et al. [24]. The asymptotic fields are essentially two-
225 dimensional in the crack front of three-dimensional cracks. Moreover, only the term $\sqrt{r}\sin(\theta/2)$ of the enrichment functions for two-dimensional problems is discontinuous. The remaining ones are intended to enhance the accurateness in linear elastic fracture
230 mechanics. This is also corroborated by Moes et al. [25].

$$\psi_k(x)|_{k=1,..,12} = [\sqrt{r}\sin(\theta/2)\cos(\varepsilon\log(r))e^{\pm\varepsilon\theta},$$
$$\sqrt{r}\cos(\theta/2)\cos(\varepsilon\log(r))e^{\mp\varepsilon\theta}, ...] \quad (8)$$

Strong form of the governing equations. The 'strong form' of the governing equations of a fractured solid –assuming negligible body forces– are presented in
235 Eqs.(9).

$$\begin{aligned} \nabla \cdot \boldsymbol{\sigma} &= \mathbf{0} \ \text{ on } \ \Omega \\ \mathbf{u} &= \tilde{\mathbf{u}} \ \text{ on } \ \Gamma_u \\ \boldsymbol{\sigma} \cdot \mathbf{n}_{\Gamma_t} &= \tilde{\mathbf{t}} \ \text{ on } \ \Gamma_t \\ \boldsymbol{\sigma} \cdot \mathbf{n}_{\Gamma_c} &= \mathbf{0} \ \text{ on } \ \Gamma_c \end{aligned} \qquad (9)$$

where Ω is the solid domain, $\tilde{\mathbf{u}}$ are the prescribed displacements in Γ_u part of the domain, $\tilde{\mathbf{t}}$ is the traction defined on Γ_t. A crack is defined by Γ_c and nor-
240 mal $\mathbf{n}_{\Gamma_c}$, see Figure 1. The two opposite faces of any crack are assumed traction free as enforced in Eqs.(9) last line.
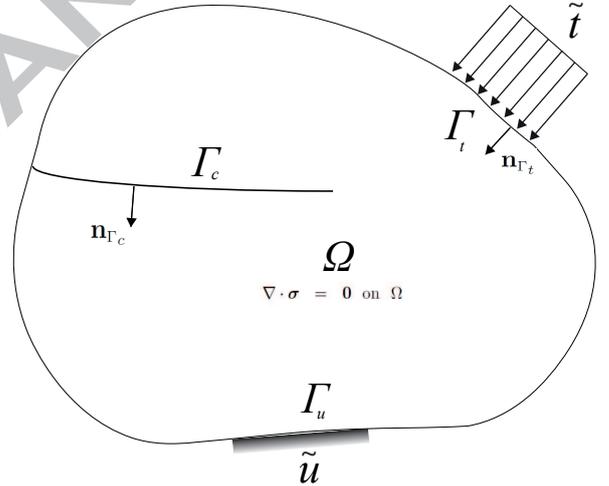
Figure 1: Schematic detail of the notation used.

Weak form of the governing equations. The weak form can be obtained by applying a Galerkin's pro-
245 cedure, i.e. multiplying the governing equation in Eqs.(9) by an admissible trial function $\boldsymbol{\delta u}(\mathbf{x})$ defined in the same domain of the approximation Eq.(10).

$$\boldsymbol{\delta u}(\mathbf{x}) = \mathbf{N}^{\mathbb{A}}(\mathbf{x}) \cdot \boldsymbol{\delta u}^{\mathbb{A}} + \mathbf{N}^{(enr)}(\mathbf{x}) \cdot \delta\mathbf{a}^{(enr)} \qquad (10)$$

Applying Galerkin's,

$$\int_{\Omega} (\nabla \cdot \boldsymbol{\sigma}) \cdot \boldsymbol{\delta u} \, \mathrm{d}\Omega = 0 \qquad (11)$$

Applying the *Divergence Theorem*, imposing the boundary conditions and allowing free traction on the
250 crack faces, renders,

4

$$\int_{\Omega} (\nabla \boldsymbol{\delta u} : \boldsymbol{\sigma}) \, \mathrm{d}\Omega + \int_{\Gamma_c} [\![\boldsymbol{\delta u}]\!] \boldsymbol{\sigma} \cdot \mathbf{n}_{\Gamma_c} \mathrm{d}\Gamma = \int_{\Gamma_t} \boldsymbol{\delta u} \cdot \tilde{\mathbf{u}} \mathrm{d}\Gamma \tag{12}$$

the second term on the left hand side of Eq.(12) cancels out due to the integrals on the two faces of the crack being with different sign and equal absolute value.

$$\int_{\Omega} (\nabla \boldsymbol{\delta u} : \boldsymbol{\sigma}) \, \mathrm{d}\Omega = \int_{\Gamma_t} \boldsymbol{\delta u} \cdot \tilde{\mathbf{u}} \mathrm{d}\Gamma \tag{13}$$

255 Eq.(13) is expressed in tensor form as follows,

$$\int_{\Omega} (\bar{\mathbf{B}}^T \cdot \boldsymbol{\sigma}) \, \mathrm{d}\Omega = \int_{\Gamma_t} \bar{\mathbf{N}}^T \cdot \tilde{\mathbf{u}} \, \mathrm{d}\Gamma \tag{14}$$

where $\bar{\mathbf{B}} = [\mathbf{B}^{\mathbb{A}}, \mathbf{B}^{(face)}, \mathbf{B}^{(front)}]$ and $\bar{\mathbf{N}} = [\mathbf{N}^{\mathbb{A}}, \mathbf{N}^{(face)}, \mathbf{N}^{(front)}]$. Any strain operator tensor $\mathbf{B}$ contains the corresponding shape function derivatives, Eq.(15):

$$\mathbf{B}_i^{(\square)} = \begin{bmatrix} N_{i,x}^{(\square)} & 0 \\ 0 & N_{i,y}^{(\square)} \\ N_{i,y}^{(\square)} & N_{i,x}^{(\square)} \end{bmatrix} \tag{15}$$

260 Note that,

$$\mathbf{N}^{(face)} = [H(\mathbf{x}) - H(\mathbf{x}_\mathbb{B})] \, \mathbf{N}^{\mathbb{B}}(\mathbf{x}) \tag{16}$$
$$\mathbf{N}^{(front)} = [\psi_k(\mathbf{x}) - \psi_k(\mathbf{x}_\mathbb{C})] \, \mathbf{N}^{\mathbb{C}}(\mathbf{x}) \tag{17}$$

Being $H(\mathbf{x})$ the Heaviside function, Eq.(18).

$$H(\mathbf{x}) = \begin{cases} +1 & \text{if } \Phi(\mathbf{x}) \geq 0 \\ -1 & \text{if } \Phi(\mathbf{x}) < 0 \end{cases} \tag{18}$$

and $\Phi(\mathbf{x})$ is a signed distance-to-crack function or level set function Osher and Sethian [26], Eq.(19).

$$\Phi(\mathbf{x}) = sign((\mathbf{x} - \mathbf{x}^{(\mathbf{face})}) \cdot \mathbf{n}_{\Gamma_c}) \, min \|\mathbf{x} - \mathbf{x}^{(\mathbf{face})}\| \tag{19}$$

where $\mathbf{x}^{(\mathbf{face})}$ is a point in the crack or discontinuity. It is usual to have the same shape functions for the sake of simplicity, see Khoei [27]. Thus, $\mathbf{N}^{\mathbb{A}} = \mathbf{N}^{\mathbb{B}} = \mathbf{N}^{\mathbb{C}}$

Discretisation. The discretisation of Eq.(14) by fi-
265 nite elements renders the system of equations Eq.(20) where numerical integration at quadrature points to approximate the integrals is performed.

$$\mathbf{K} \cdot \mathbf{U} = \mathbf{F} \tag{20}$$

where $\mathbf{K}$ is the global stiffness matrix, $\mathbf{U} = [\mathbf{u}^{\mathbb{A}}, \boldsymbol{d}^{\mathbb{B}}, \boldsymbol{b}^{\mathbb{C}}]$ is the vector of unknowns and $\mathbf{F}$ and is the nodal external forces vector.

$$\begin{bmatrix} \mathbf{K_{uu}} & \mathbf{K_{ud}} & \mathbf{K_{ub}} \\ \mathbf{K_{du}} & \mathbf{K_{dd}} & \mathbf{K_{db}} \\ \mathbf{K_{bu}} & \mathbf{K_{bd}} & \mathbf{K_{bb}} \end{bmatrix} \cdot \begin{Bmatrix} \mathbf{u}^{\mathbb{A}} \\ \boldsymbol{d}^{\mathbb{B}} \\ \boldsymbol{b}^{\mathbb{C}} \end{Bmatrix} = \begin{Bmatrix} \mathbf{F_u} \\ \mathbf{F_d} \\ \mathbf{F_b} \end{Bmatrix} \tag{21}$$

where,

$$\mathbf{K_{uu}} = \int_{\Omega} [\mathbf{B}^{\mathbb{A}}]^{\mathbf{T}} \cdot \mathbf{D} \cdot \mathbf{B}^{\mathbb{A}} \mathrm{d}\boldsymbol{\Omega}$$
$$\mathbf{K_{ud}} = \int_{\Omega} [\mathbf{B}^{\mathbb{A}}]^{\mathbf{T}} \cdot \mathbf{D} \cdot \mathbf{B}^{(\mathbf{face})} \mathrm{d}\boldsymbol{\Omega}$$
$$\mathbf{K_{ub}} = \int_{\Omega} [\mathbf{B}^{\mathbb{A}}]^{\mathbf{T}} \cdot \mathbf{D} \cdot \mathbf{B}^{(\mathbf{front})} \mathrm{d}\boldsymbol{\Omega}$$
$$\mathbf{K_{du}} = \int_{\Omega} [\mathbf{B}^{(\mathbf{face})}]^{\mathbf{T}} \cdot \mathbf{D} \cdot \mathbf{B}^{\mathbb{A}} \mathrm{d}\boldsymbol{\Omega}$$
$$\mathbf{K_{dd}} = \int_{\Omega} [\mathbf{B}^{(\mathbf{face})}]^{\mathbf{T}} \cdot \mathbf{D} \cdot \mathbf{B}^{(\mathbf{face})} \mathrm{d}\boldsymbol{\Omega}$$
$$\mathbf{K_{db}} = \int_{\Omega} [\mathbf{B}^{(\mathbf{face})}]^{\mathbf{T}} \cdot \mathbf{D} \cdot \mathbf{B}^{(\mathbf{front})} \mathrm{d}\boldsymbol{\Omega}$$
$$\mathbf{K_{bu}} = \int_{\Omega} [\mathbf{B}^{(\mathbf{front})}]^{\mathbf{T}} \cdot \mathbf{D} \cdot \mathbf{B}^{\mathbb{A}} \mathrm{d}\boldsymbol{\Omega}$$
$$\mathbf{K_{bd}} = \int_{\Omega} [\mathbf{B}^{(\mathbf{front})}]^{\mathbf{T}} \cdot \mathbf{D} \cdot \mathbf{B}^{(\mathbf{face})} \mathrm{d}\boldsymbol{\Omega}$$
$$\mathbf{K_{bb}} = \int_{\Omega} [\mathbf{B}^{(\mathbf{front})}]^{\mathbf{T}} \cdot \mathbf{D} \cdot \mathbf{B}^{(\mathbf{front})} \mathrm{d}\boldsymbol{\Omega}$$

$\mathbf{D}$ is the constitutive matrix containing the material
270 properties. The vector of nodal external forces components are calculated by numerical integration of the following integrals,

$$\mathbf{F_u} = \int_{\Gamma_t} [\mathbf{N}^{\mathbb{A}}]^{\mathbf{T}} \cdot \mathbf{t} \, \mathrm{d}\boldsymbol{\Gamma}$$
$$\mathbf{F_d} = \int_{\Gamma_t} [\mathbf{N}^{(\mathbf{face})}]^{\mathbf{T}} \cdot \mathbf{t} \, \mathrm{d}\boldsymbol{\Gamma}$$
$$\mathbf{F_b} = \int_{\Gamma_t} [\mathbf{N}^{(\mathbf{front})}]^{\mathbf{T}} \cdot \mathbf{t} \, \mathrm{d}\boldsymbol{\Gamma}$$

Evaluation of J-integral. The energy release rate (ERR) whereby the transversal crack advances based on the J-integral is calculated with Eq.(22). This equation is computed using the elements around the crack front that are crossed by a circle centred at the crack tip and of a relevant radius to include the elements subjected to the special stress field around the crack front as depicted in Figure 2. As opposed to standard FEM, XFEM enriches the nodes around the crack with adequate enrichment functions based

5

on Fracture Mechanics theory (see below for these functions) whereby the J-integral computation is enhanced. Thus, the J-integral is implemented at eight quadrature points within the high-order quadrilateral finite elements as follows,

$$J = \sum_{\Omega_e^{(ctour)}} \sum_{p \subset \mathcal{N}^{(nquad)}} \left[\left(\boldsymbol{\sigma}_{ij} \frac{\partial \mathbf{u}_1}{\partial x_i} - W \delta_{1i} \right) \frac{\partial q}{\partial x_j} det \left| \frac{\partial x_k}{\partial \eta_k} \right| \right]_p w_p$$

(22)
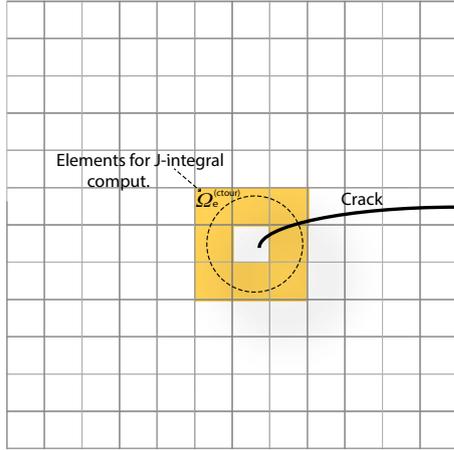
Figure 2: Generic representation of elements for J-integral computation

where q is a weighting function defined on the integral domain valued between 0 and 1, see Figure(3). $\Omega_e^{(ctour)}$ is the set of elements on the area of the integral contour, $\mathcal{N}^{(nquad)}$ is the number of quadrature per element, p denotes a quadrature point within the element, e.g. Gauss point, w_p is the weight associated to the quadrature point p for numerical integration, and,

$$\frac{\partial q}{\partial x_j} = \sum_{I \subset \mathcal{N}^{(nnodes)}} \frac{\partial N_I}{\partial \eta_k} \frac{\partial \eta_k}{\partial x_j} q_I \quad j = 1, 2$$

(23)

where $\mathcal{N}^{nnodes}$ is the number of nodes per element, N_I denote shape functions. $\frac{\partial \eta_k}{\partial x_j}$ is the inverse Jacobian matrix of transformations.

3. Cross-ply laminate $[0^o, 90^o]_s$ fracture

This test shows the computation of energy release rates with crack propagation in a cross-ply laminate by means of the formulation presented above. Comparison with results obtained by París et al. [28] with the Boundary Element (BEM) using the Virtual Crack Closure Technique (VCCT) [29] is carried out. The configuration –depicted in Figure 4– is
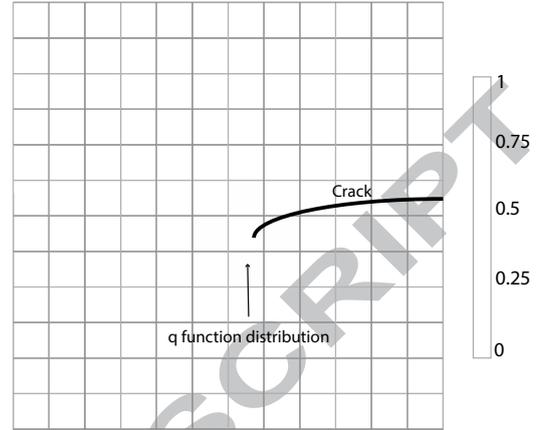
Figure 3: Generic representation of weighting function q

a cross-ply carbon epoxy laminate (AS4/8552 Hexcel) $[0^o, 90^o]_s$, with mechanical properties given in Table(1), subjected to traction perpendicular to the $[90^o]$ lamina and longitudinally to $[0^o]$ lamina. Details of the geometry, loading and qualitatively representation of the cracks occurring in a regular pattern, i.e. separated approximately a distance 2L as found on experimental works by París et al. [28] is schematically depicted in Figure 4. The correlation between the distance between transverse cracks 2L and the dimensions L in cross-ply laminate has been pointed out in París et al. [30].
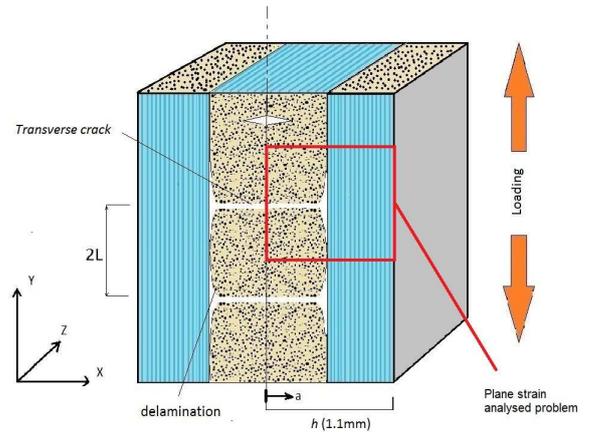
Figure 4: Schematic representation of transversal cracks and delamination in [0/90]s laminate.

The problem can be reduced to a plain strain state simplifying significantly the computational task. The

6

dimensions are $2t \times 2L$ where $t = 0.55\,mm$ is the thickness of half of 90^0 laminae and also the thickness of any of the two 0^0 plies. Thus, the laminate is prone to develop a transversal crack that eventually triggers delamination when it is nearby the interface $[0^0, 90^0]$. An analytical solution for the energy release rate with the crack progression has been formulated by McCartney [31].

Elastic properties	Value
Young's Modulus in fibre direction, E_{11}	$141.3\,GPa$
Young's Moduli (normal-to-fibre), E_{22}, E_{33}	$9.58\,GPa$
Poisson's Ratio, ν_{23}	0.32
Poisson's Ratios, ν_{12}, ν_{13}	0.3
Shear Modulus (plane normal-to-fibres), G_{23}	$3.5\,GPa$
Shear Moduli, G_{12}, G_{13}	$5\,GPa$

Table 1: Material properties of carbon epoxy laminate AS4/8552 Hexcel
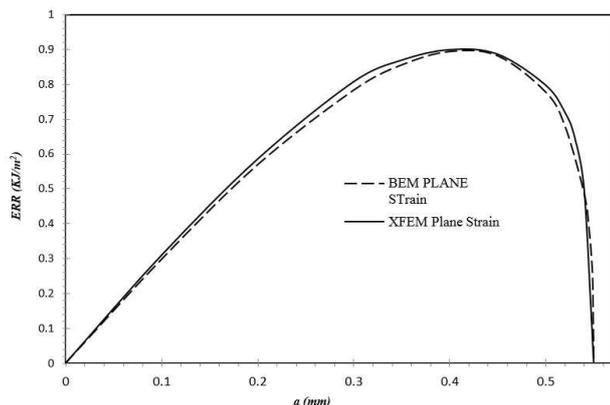
Figure 5: Energy release rates with the advancement of the transversal crack (a - length) in the cross-ply laminate. Comparison between XFEM output and the result obtained by París et al. [28] with the Boundary Element Method (BEM)

Figure 5 shows the ERR with the propagation of the transversal crack perpendicularly to the loading direction. It is remarkable that the ERR vanishes when the transverse crack is getting close to the interface. This may be explained by the presence of the near interface to the final crack tip. This is also corroborated by a sudden increment on the interfacial stress Figure 6 responsible for creating eventually delamination in the interface. Figure 6 depicts the distribution of normal stress at the interface for three distinct crack lengths showing clearly this trend of increasing stress with the proximity of the transverse crack to the interface. The delamination crack

would start in the intersection between the interface and a virtual longitudinal projection of the transverse crack. This is in agreement with the experimental evidence by París et al. [30]. Furthermore, it makes sense from a theoretical point of view as stated by Lu and Erdogan [32]. This ascertained that when a crack evolving in the softer material –in this case the 90^0 plies, i.e. the crack running through the resin continuum and disbonding between fibres and matrix– is approaching a tougher interface the ERR drops suddenly up to vanishing.
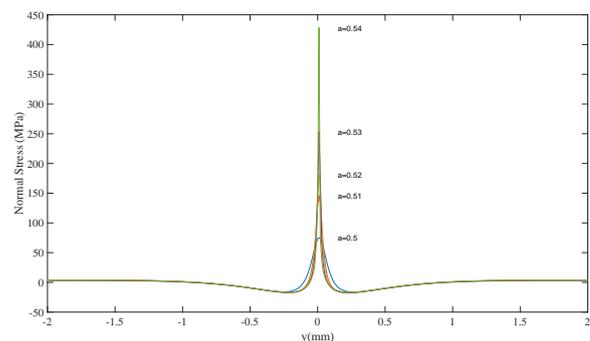
Figure 6: Normal stress along the interface at different transversal crack lengths

4. Delamination on hybrid composite DCB

This test aims to model the mode I fracture of double cantilever beam (DCB) made of an asymmetric hybrid composite with a $\{0^0/90^0\}$ interface located at mid-thickness. The DCB sample is made of two $4.5\,mm$ thick layers of Aluminium with a core made of two composite plies with a $\{0^0/90^0\}$ interface of $0.01\,mm$ thickness. This test assumes a pre-notched specimen following ASTM standards and the application of load perpendicular to the longitudinal axis of the sample to gradually open a neat crack that runs in the $\{0^0/90^0\}$ interface of toughness $3.5\,kJ/m^2$. The opposite edge is rigidly clamped, i.e. the displacements are fully constrained. The composite laminate consists of a stacking sequence $[Al/0^0/90^0/Al]$. The material properties of the composite plies are: $E_{11} = 53980\,N/mm^2, E_{22} = 9412\,N/mm^2, E_{33} = 9412\,N/mm^2, \nu_{12} = 0.33, \nu_{13} = 0.33, \nu_{23} = 0.33, G_{12} = 5548\,N/mm^2, G_{13} = 3000\,N/mm^2, G_{23} = 5548\,N/mm^2$. The loading versus opening displacement with evolving crack is compared with experimental tests [33], see Figure 7. The

present approach was able to capture the propagation of the crack closely matching the experimental output as well as the instant, i.e. level of loading, at which the crack is initiated. Figure 8 depicts the opening displacement versus delamination. The initiation criterion was based on the maximum strength of the interface. Once this is reached a crack is originated and allowed to evolved based upon the energy release.
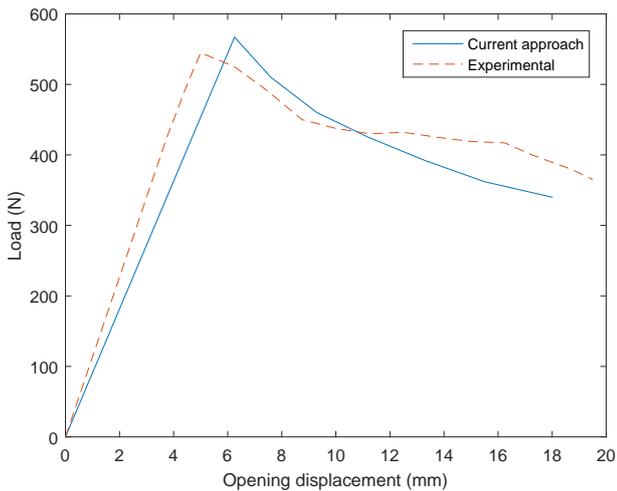
Figure 7: Delamination in $\{0^0/90^0\}$ interface: loading vs. opening displacement
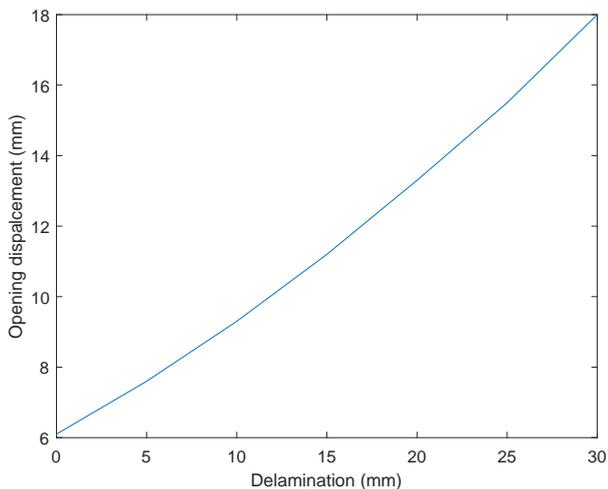
Figure 8: Delamination in $\{0^{0/90^0}\}$ interface: displacement vs. delamination

5. Conclusion

This article has presented a study to simulate fracture and delamination in composite laminates based on the partition of finite elements. It has shown the evolution of the energy release rate in a cross-ply laminate. This has been approached for the first time by means of the Extended Finite Element Method based on special enrichment and computation of energy release rate. The formulation used for the implementation in a software platform has been shown in detail with special attention to those features necessary for modelling discontinuities in composite structures. Furthermore, the computation of the energy release rate with XFEM is provided without re-meshing needed which constitutes an advance respect to classical formulations with FEM. The investigation with the proposed numerical scheme on $[0^0, 90^0]_s$ laminates resulted in the following:

- The energy release rate follows a similar pattern to that observed with other methodologies, e.g. Boundary Element Method as depicted in Figure 5. However, the fact that re-meshing is not necessary in the present approach reduces naturally the computational cost.

- The energy release rate decreases suddenly after a peak value of $0.9\,kJ/m^2$ at approximately $0.15mm$ from the $\{0^0/90^0\}$ interface.

- The progressive increment of interfacial stress in the $\{0^0, 90^0\}$ interface, eventually delaminating such interface, induced the ERR reduction due to the transversal crack running across the 90^0 plies up to vanishing.

In addition, the analysis of delamination associated to mode I fracture of an asymmetric hybrid composite with a $\{0^0/90^0\}$ interface located at mid-thickness evidenced an adequate correlation between the current approach and the experimental tests. Ongoing effort is pointing towards the implementation for woven composites in which enrichment must be tailored for purpose and particular configurations are presenting certain drawbacks such as convergence when dealing with complex composite systems.

References

[1] Liu P.F., Zheng J.Y. Recent developments on damage modeling and finite element analysis for composite laminates: A review. Materials and Design, 2010;31(8):3825–34.

[2] Curiel Sosa J., Phaneendra S., Munoz J. Modelling of mixed damage on fibre reinforced composite laminates subjected to low velocity impact. International Journal of Damage Mechanics, 2013;22:356–74.

8

[3] Matzenmiller A., Lubliner J., Taylor R. A constitutive model for anisotropic damage in fiber-composites. Mech Mater, 1995;20:125–52.

[4] van Dongen B., van Oostrum A., Zarouchas D. A blended continuum damage and fracture mechanics method for progressive damage analysis of composite structures using xfem. Composite Structures, 2018;184:512–22.

[5] Turon A., Gonzlez E., Sarrado C., Guillamet G., Maim P. Accurate simulation of delamination under mixed-mode loading using a cohesive model with a mode-dependent penalty stiffness. Composite Structures, 2018;184:506–11.

[6] Iarve E.V., Gurvich M.R., Mollenhauer D.H., Rose C.A., Dávila C.G. Mesh-independent matrix cracking and delamination modeling in laminated composites. International Journal for Numerical Methods in Engineering, 2011;88(8):749–73.

[7] Zhao L., Zhi J., Zhang J., Liu Z., Hu N. Xfem simulation of delamination in composite laminates. Composites Part A: Applied Science and Manufacturing, 2016;80:61–71.

[8] Abdullah N., Curiel-Sosa J., Taylor Z., Tafazzolimoghaddam B., Martinez Vicente J., Zhang C. Transversal crack and delamination of laminates using xfem. Composite Structures, 2017;173:78–85.

[9] Navarro-Zafra J., Curiel-Sosa J., Serna Moreno M. Mixed-mode damage into a cgrp cruciform subjected to biaxial loading. Composite Structures, 2015;133(1093-1100).

[10] Turon A., Camanho P.P., Costa J., Dvila C.G. A damage model for the simulation of delamination in advanced composites under variable-mode loading. Mechanics of Materials, 2006;38(11):1072–89.

[11] Shi G., Zhang H., Wang J., Wang Z. Progressive delamination simulation of laminated plates based on a solid-shell interface element with damage-node model. Procedia Engineering, 2012;31:324–30.

[12] Hallett S.R., Jiang W.G., Khan B., Wisnom M.R. Modelling the interaction between matrix cracks and delamination damage in scaled quasi-isotropic specimens. Composites Science and Technology, 2008;68(1):80–9.

[13] Tay T.E., Sun X.S., Tan V.B.C. Recent efforts toward modeling interactions of matrix cracks and delaminations An integrated XFEM-CE approach. Advanced Composite Materials, 2014;23:391–408.

[14] Serna Moreno M., Curiel-Sosa J., Navarro-Zafra J., Martinez Vicente J., Lopez Cela J. Crack propagation in a chopped glass-reinforced composite under biaxial testing by means of xfem. Composite Structures, 2014;119:264–71.

[15] Dimitri R., Fantuzzi N., Li Y., Tornabene F. Numerical computation of the crack development and sif in composite materials with xfem and sfem. Composite Structures, 2017;160:468–90.

[16] Zhao L., Wang Y., Zhang J., Gong Y., Hu N., Li N. Xfem-based model for simulating zigzag delamination growth in laminated composites under mode i loading. Composite Structures, 2017;160:1155–62.

[17] Hansbo A., Hansbo P. A finite element method for the simulation of strong and weak discontinuities in solid mechanics. Comput Methods Appl Mech Eng, 2004;193:3523–40.

[18] van der Meer F.P., Sluys L.J. Mesh-independent modeling of both distributed and discrete matrix cracking in interaction with delamination in composites. Engineering Fracture Mechanics, 2010;77(4):719–35.

[19] Hu X.F., Chen B.Y., Tirvaudey M., Tan V.B.C., Tay T.E. Integrated xfem-ce analysis of delamination migration in multi-directional composite laminates. Composites Part A: Applied Science and Manufacturing, 2016;90:161–73.

[20] Belytschko T., Liu W., Moran B., Elkhodary K. Nonlinear Finite Elements for Continua and Structures. Wiley; 2^{nd}ed.; , 2013.

[21] Ibbett J., Tafazzolimoghaddam B., Delgadillo H.H., Curiel-Sosa J. What triggers a microcrack in printed engineering parts produced by selective laser sintering on the first place? Materials & Design, 2015;88:588 –97.

[22] Belytschko T., Möes N., Usui S., Parimi C. Arbitray discontinuities in finite elements. Int J Numer Methods Eng, 2001;50:993–1013.

[23] Curiel Sosa J., Karapurath N. Delamination modelling of glare using the extended finite element method. Composites Science and Technology, 2012;72:788–91.

[24] Wang Z., Yu T., Bui T., Tanaka S., Zhang C., Hirose S., et al. 3-d local mesh refinement xfem with variable-node hexahedron elements for extraction of stress intensity factors of straight and curved planar cracks. Computer Methods in Applied Mechanics and Engineering, 2017;313:375 – 405.

[25] Moes N., Gravouil A., Belytschko T. Non-planar 3d crack growth by the extended finite element and level sets part i: Mechanical model. Int J Numer Methods Engrg, 2002;53:2549–68.

[26] Osher S., Sethian J. Fronts propagating with curvature dependent speed: algorithms based on hamilton-jacobi formulations. J Comput Phys, 1988;79:12–49.

[27] Khoei A. Extended Finite Element Method, Theory and Applications. Series in Computational Mechanics; Wiley; , 2015.

[28] París F., Blázquez A., L.N. M., Mantic V. Characterization and evolution of matrix and interface related damage in $[0/90]_s$ laminates under tension. part i: Numerical predictions. Composites Science and Technology, 2010;70(7):1168–75.

[29] Krueger R. Virtual crack closure technique: History, approach and applications. Appl Mechs Rev, 2004;57(1-6):109–43.

[30] París F., Blázquez A., L.N. M., Barroso A. Characterization and evolution of matrix and interface related damage in $[0/90]_s$ laminates under tension. part ii: Experimental evidence. Composites Science and Technology, 2010;70:1176–83.

[31] McCartney L.N. Predicting transverse crack formation in cross-ply laminates. Composites Science and Technology, 1998;58(7):1069–81.

[32] Lu M., Erdogan F. Stress intensity factors in two bonded elastic layers containing cracks perpendicular to and on the interface ii. solution and results. Eng Fract Mech, 1983;18:507–28.

[33] Airoldi A., Vesco M., van der Zwaag S., Baldi A., Sala G. Damage in glare laminates under indentation loads: experimental and numerical results. In: Proceedings of the 17th International Conference on Composite Materials; vol. 29:D5:10. 2009,.